Vibrational analysis and material ageing of fibre-reinforced plastics

Tommy Öhman

Degree Thesis

Plastteknik

2016

DEGREE THESIS	
Arcada	
Degree Programme:	Plastteknik
Identification number:	14071
Author:	Tommy Öhman
Title:	Vibrational analysis and material ageing of fibre-reinforced plastics
Supervisor (Arcada):	Rene Herrmann
Commissioned by:	

Abstract:
In this thesis the fatigue behaviour of a carbon/glass fibre laminate was studied. The main focus was to use acoustic vibrational analysis as a method of measuring the material ageing as well as identifying the damage growth and damage differences between 2D and 3D laminates. Four rectangular specimens were prepared of which two had been sewed together with cotton thread in the z-direction to form a 3D-laminate. The specimens were aged with constant amplitude three-point bending at different levels of strain and acoustic vibrational tests were made at regular intervals using a cantilever setup to plot the damage growth over time. The results showed that the quality factor accurately measures the ageing of a material with regular acoustic vibrational test. The addition of fibres in the z-direction was proven to slow down spreading and growth of damage in the laminate. Analysing the surface of the laminates revealed visible damage from delamination, buckling and fibre brakeage. The number of cycles were concluded to be too few to accurately draw conclusions about the late stage fatigue life and prediction of material failure of the specimens.

Keywords:	Vibration, material ageing, fibre-reinforced plastic, composite, three-point bending, acoustic testing, fatigue, 3D-laminate.
Number of pages:	49
Language:	English
Date of acceptance:	28.04.2016

EXAMENSARBETE	
Arcada	
Utbildningsprogram:	Plastteknik
Identifikationsnummer:	14071
Författare:	Tommy Öhman
Arbetets namn:	Viskoelastisk dämpning och hysteres i komposita material
Handledare (Arcada):	Rene Herrmann
Uppdragsgivare:	

Sammandrag:
I det här slutarbetet undersöktes utmattningsbeteendet av ett kolfiber/glasfiber laminat. Arbetets fokus låg på användandet av akustisk vibrationsanalys som en metod för att bestämma åldringsförfarandet och skadeutvecklingen av materialet, samt skillnader mellan 2D och 3D laminat i dessa syften. Fyra rektangulära testbitar tillverkades, varav två hade blivit ihopsydda med bomullstråd i z-riktningen för att skapa ett 3D laminat. Dessa testbitar åldrades genom trepunktsböjning med konstant böjningsamplitud vid två olika deformationer och akustiska vibrationstest gjordes regelbundet under tiden för att kartlägga skadeutvecklingen. Vibrations testen ufördes på så sätt att testbitarna var fastspännda endast i ena ändan. Resultaten tydde på att godhetstalet kan användas för att bestämma skadeutvecklingen i ett material genom regelbundna vibrationstest. Det kunde även fastställas att fibrer i z-riktningen motverkar att skador i laminatet kan växa och spridas. Vid analys av de synliga skadorna kunde det konstateras att även skador i form av separering av lager, knäckningsskador och brustna fibersträngar har förekommit. Det kunde även konstateras att antalet böjningar var för få för att på ett trovärdigt sätt kunna dra slutsatser om hur materialet kommer att utmattas hädanefter eller när och hur materialet kommer att gå sönder.

Nyckelord:	Vibration, åldring av material, fiber, komposit, trepunktsböjning, akustiska test, utmattning, 3D laminat.
Sidantal:	49
Språk:	Engelska
Datum för godkännande:	28.04.2016

CONTENTS

Figures

Tables

LIST OF SYMBOLS AND ABBREVIATIONS

2D	two dimensional
3D	three dimensional
b	width
c	viscous damping coefficient
δ	logarithmic decrement
Δf	half-power bandwidth
E	modulus of elasticity
ε	strain
F	force
F_μ	friction force
f	frequency
f_r	resonance frequency
FEM	finite element method
FRP	fibre-reinforced polymer
ζ	damping ratio
h	thickness
I	area moment of inertia
k	spring constant
L	length
m	mass
μ	mass per unit length
Q	quality factor
σ	stress
t	time
T_d	damped period
x	distance or point
y	displacement
ω_d	damped natural frequency
ω_n	natural frequency

1 INTRODUCTION

1.1 Background

The purpose of this thesis is to investigate the possibility of a non-destructive testing method for measuring the ageing and prediction of material failure of fibre-reinforced plastics (FRP). A FRP subjected to cyclic loading will cause initiation and growth of microscopic (and macroscopic) damage in the material. The hypothesis stand that this damage growth would be measureable as a decrease of the quality factor, with the assumption that the quality factor is a direct measurement of the ageing of a material. The most relevant research question is therefore to prove the correlation between ageing and the quality factor and determine if the change over time can be measured using regular acoustic vibrational tests. If the hypothesis would stand correct, it would make possible for on-site acoustic vibrational testing, which would enable better monitoring of the condition of laminates and more accurate predictions for material failure of FRP parts.

The fatigue behaviour of FRPs have become a popular subject for research as the growing composite industry demands increasingly better and more accurate means of predicting the fatigue life of its products. Damage accumulation to FRPs have been documented widely and studies made by Xue et al. (Xue, et al., 2015), Ajaja & Barthelat (Ajaja & Barthelat, 2016) and Sudevan et al. (Sudevan, et al., 2015), among others, point toward that the damage growth of FRPs follow characteristic trends that may be modelled and likely also accurately predicted. The fatigue testing are usually performed using cyclic three-point bending and a frequently occurring problem is that the testing speed is too low to reach the high number of cycles often required to accurately define the complete fatigue life in a reasonable time. Xue et al. (Xue, et al., 2007) and Backe et al. (Backe, et al., 2015) have developed setups for cyclic three-point bending that allows for testing speeds up to 20 kHz to counter this problem, which are expected to aid the study of fatigue behaviour of composites at very high cycle fatigue.

The demand for non-destructive testing methods for damage identification in FRPs is apparent, as there is a lot of research on this matter with various different approaches to the subject. The purpose of these studies are generally to develop a method capable of

identifying damage in an early stage to predict and prevent material failure and enhance the service life of FRP parts. Numerous studies have been made using vibrational testing as an alternative non-destructive testing method. Experimental researches have been made by Perez et al., Lakhdar et al., Kersemans et al. and Klepka et al. focusing on both visible and barely visible damage as well as identification and localisation of damage growth. Studies focusing on mathematically modelling the fatigue life are common as well, for example studies by Zhang et al. (Zhang, et al., 2013) and Yan et al. (Yan, et al., 2006) focusing on optimisation of FEM analysis and the importance of correct meshing to form a method of accurately predicting the damage accumulation in FRPs without experimental tests.

A trend among these studies are that most claim to have promising results but all recommend further study to prove their theories, which indicates that this subject may still be a work in progress. An article by Yan et al. (Yan, et al., 2007) about the development of vibration-based methods for damage identification, support this statement by stating that vibrational testing are on the rise but still have its limitations. Most studies focus on the relation of stiffness degradation and damage accumulation, while none of the researches mentioned use the quality factor in their research. These statements should consequently justify further research on the subject of fatigue behaviour and identification of damage growth in FRPs with the use of vibrational analysis, especially in relation to the quality factor.

1.2 Objectives

The main objectives of this thesis are (I) to prove the correlation between the ageing of a material and the quality factor, (II) determine if regular acoustic vibrational tests may be used as a method of measuring the damage growth and (III) predicting the fatigue life of fibre-reinforced plastics. This thesis also seeks (IV) to prove that the addition of fibres in the z-direction will resist damage from spreading across the laminate. A secondary objective of this thesis is (V) to identify the failure mode(s) of FRPs as a result of ageing.

2 LITTERATURE REVIEW

2.1 Theory

2.1.1 Free vibration

Free vibrations occur when a spring system is subjected to an initial kinetic energy or initial displacement from the equilibrium position that leads to potential energy in the system. This will make the system oscillate about its equilibrium position. If no external forces acts upon the system, the oscillating motion is referred to as free vibration. A cantilever beam may be modelled as a spring system if the mass of the beam is seen as a concentrated weight at the free end of the beam and the beam itself is considered to be equivalent of a spring, as illustrated in Figure 1. (Kelly, 2011, p. 137) (Thomson, 1996, p. 17)

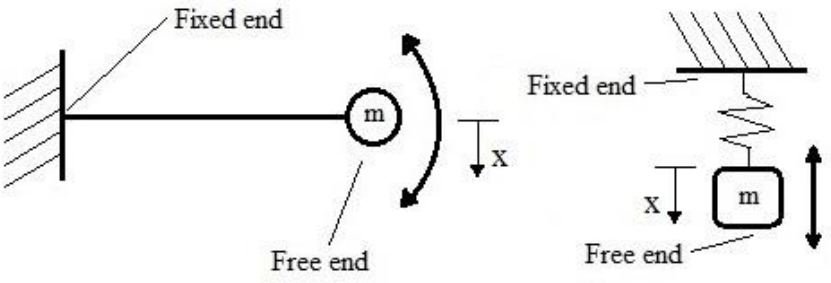

Figure 1 Schematic drawing of a cantilever beam modelled as a spring system.

The second-order differential equation for any single degree of freedom system is (Kelly, 2011, pp. 138-139) (Thomson, 1996, pp. 28-30)

$$m\ddot{x} + c\dot{x} + kx = F(t) \qquad \textit{Equation 1}$$

Since no force is acting upon the system $F(t) = 0$ and the system parameters are defined as

$$\omega_n = \sqrt{\frac{m}{k}} \quad and \quad \zeta = \frac{c}{2\sqrt{km}} \qquad \textit{Equation 2 \& 3}$$

the equation become

$$\ddot{x} + 2\zeta\omega_n\dot{x} + \omega_n^2 x = 0 \qquad \textit{Equation 4}$$

where ω_n is the natural frequency and ζ is the damping ratio.

A solution for equation 4 may be assumed to be

$$x(t) = Ae^{\alpha t} \qquad \textit{Equation 5}$$

because of the linearity and constant coefficients in the equation. If substituting equation 5 into equation 4 it yields

$$(\alpha^2 + 2\zeta\omega_n\alpha + \omega_n^2)Ae^{\alpha t} = 0 \qquad \textit{Equation 6}$$

The solution may then be obtained by solving for the roots, which give the two roots

$$\alpha = \omega_n\left(-\zeta \pm \sqrt{\zeta^2 - 1}\right) \qquad \textit{Equation 7}$$

The solution varies with the value of the damping ratio. There are four different possibilities, if setting $i = \sqrt{-1}$ the possibilities are: (Kelly, 2011, pp. 140, 147-160) (Thomson, 1996, pp. 29-33)

1. Undamped $\zeta = 0$

   In theory if there was no damping the free vibration would be a continuous harmonic oscillating motion, in practice however some form of damping is present in all vibrations.

   $$\alpha = \pm i\omega_n$$

2. Underdamped $0 < \zeta < 1$

   If the damping ratio is less than one but more than zero the vibrations are underdamped and will die out with a decaying oscillating motion. The underdamped case is the case relevant for this study and will be explained further later on. Neither of the roots are real in this case and consist of complex conjugates.

   $$\alpha = \omega_n\left(-\zeta \pm i\sqrt{1 - \zeta^2}\right)$$

3. Critically damped $\zeta = 1$

   If the damping ratio equals one there is no oscillatory motion, but instead the system returns to equilibrium instantly. In this case only one of the roots are real.

   $$\alpha = -\omega_n$$

4. Overdamped $\zeta > 1$

   If the damping ratio is greater than one the vibrations are heavily damped and will without oscillating return to equilibrium slowly. In this case both roots are real.

   $$\alpha = \omega_n\left(-\zeta \pm \sqrt{\zeta^2 - 1}\right)$$

The general solution for underdamped vibration is defined as (Kelly, 2011, pp. 147-148) (Thomson, 1996, p. 29)

$$x(t) = C_1 e^{\left(-\zeta\omega_n - i\omega_n\sqrt{1-\zeta^2}\right)t} + C_2 e^{\left(-\zeta\omega_n + i\omega_n\sqrt{1-\zeta^2}\right)t} \quad \textit{Equation 8}$$

where C_1 and C_2 are constants determined from the initial conditions. Equation 8 may also be expressed as

$$x(t) = e^{-\zeta\omega_n t}[C_1\, cos(\omega_d t) + C_2\, sin(\omega_d t)] \quad \textit{Equation 9}$$

where ω_d is the damped natural frequency and is defined as

$$\omega_d = \omega_n\sqrt{1-\zeta^2} \quad \textit{Equation 10}$$

In an underdamped system the vibrations will decrease in strength with time, but the time between each cycle will be constant. This time is referred to as the damped period, T_d, and is expressed as (Kelly, 2011, p. 148) (Thomson, 1996, p. 33)

$$T_d = \frac{2\pi}{\omega_d} \quad \textit{Equation 11}$$

The decrease in strength of vibrations over time in an underdamped system is referred to as the logarithmic decrement, δ, and may be determined in several ways

$$\delta = \frac{1}{n} ln\left(\frac{x(t)}{x(t+nT_d)}\right) = \zeta\omega_n T_d = \frac{2\pi\zeta}{\sqrt{1-\zeta^2}} \quad \textit{Equation 12}$$

The damping ratio may be calculated from the logarithmic decrement as (Kelly, 2011, pp. 149-150) (Thomson, 1996, p. 33)

$$\zeta = \frac{\delta}{\sqrt{4\pi^2+\delta^2}} \quad \textit{Equation 13}$$

2.1.2 Viscous damping

If a system vibrates in a fluid medium, such as air or water, energy will be lost due to the resistance the medium puts on the vibrating body. This will cause the vibrations to decay exponentially as explained in the previous paragraph. The degree of viscous damping depends on several factors, namely the viscosity of the liquid, but also the shape and size of the body, frequency and velocity of vibrations. The damping force due to viscous damping is proportional to the velocity of the vibrating body. (Kelly, 2011, pp. 71-73)

$$F = -c\dot{x} \quad \textit{Equation 14}$$

2.1.3 Hysteretic damping

Damping caused by the material itself is referred to as hysteretic damping or structural damping and will show in the stress-strain curve as a loop as illustrated in Figure 2. For an ideal material the stress-strain curve of a loading-unloading cycle would be linear, due to no energy lost in the process. In reality however, intermolecular layers may slide and molecular bonds may brake and cause friction, which as a result may cause microscopic damage or imperfections in the material to grow as the strain energy in the material is dissipated as thermal energy. The energy dissipated may be referred to as ageing of the material and the process is irreversible. The energy lost each cycle is proportional to the square of the initial amplitude, while the frequency is known to have no effect on the energy lost per cycle. (Kelly, 2011, pp. 167-169) (Thomson, 1996, p. 75)

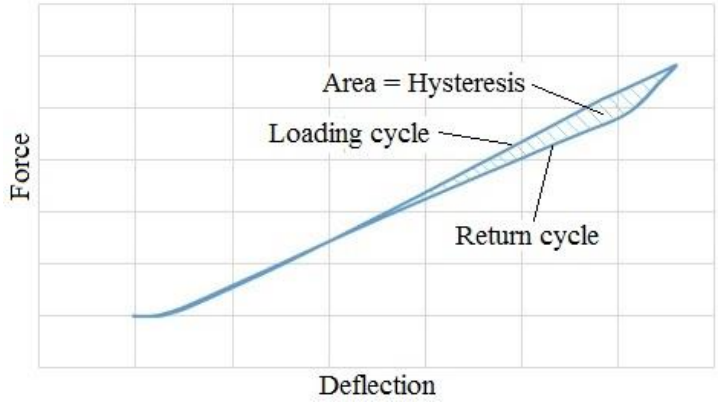

Figure 2 Example of a typical hysteresis loop.

2.1.4 Frictional damping

Frictional damping is also known as Coulomb damping and is a results of two dry surfaces sliding against each other generating a friction force, F_μ, that resists the motion. Frictional damping may originate from friction of macroscopic damage such as delamination, contrary to friction from microscopic damage, which will result in hysteretic damping. Therefore an undamaged FRP may have no frictional damping present, but may develop it as the material ages. The damping force due to friction is proportional to the friction coefficient times the normal force and the sign is the opposite of the velocity. Unlike viscous damping, frictional damping generates a constant decay of vibrations. (Kelly, 2011, pp. 160-164) (Thomson, 1996, pp. 35-36)

$$m\ddot{x} + kx = -F_\mu mg \qquad \textit{Equation 15}$$

2.1.5 Free vibration of a cantilever beam with distributed mass

To model the free vibrations of a cantilever beam a few assumptions have to be made. First the composite beam is assumed to be a uniform thin beam and in addition to that it is assumed that no rotary inertia or shear forces act upon the beam as well as no damping. The displacement, y, of the beam is then modelled, using a fourth order partial differential equation, as a function of point, x, and time, t. (Capozucca, 2014, pp. 212-213) (Safa, et al., 2011, pp. 2-5)

$$EI\frac{\partial^4 y}{\partial x^4} + \mu\frac{\partial^2 y}{\partial t^2} = 0 \qquad \textit{Equation 16}$$

Where E is the modulus of elasticity of the material, I is the area moment of inertia of the cross-section of the beam and μ is the mass per unit length.

The fourth order partial differential equation may then be reduced to a fourth order ordinary differential equation using the solution. Since the solution is expected to be a harmonic function of time the solution must have the form of

$$y(x,t) = Y(x)sin(\omega t + \alpha) \quad or \quad y(x,t) = Y(x)\,cos(\omega t + \alpha) \qquad \textit{Equation 17}$$

and if inserting equation 17 into equation 16 the following fourth order ordinary differential equation is obtained

$$\frac{d^4Y}{dx^4} + \lambda^4 Y = 0 \qquad \textit{Equation 18}$$

where

$$\lambda^4 = \frac{\mu\omega_n^2}{EI} \qquad \textit{Equation 19}$$

The general solution to equation 18 is

$$Y(x) = C_1\,sin\,\lambda x + C_2\,cos\,\lambda x + C_3\,sinh\,\lambda x + C_4\,cosh\,\lambda x \qquad \textit{Equation 20}$$

where the constants $C_1,\ C_2,\ C_3\ and\ C_4$ may be determined from the boundary conditions.

A cantilever beam have one end fixed and the other end free as schematically illustrated in Figure 3. For a cantilever beam with distributed mass, meaning that the mass is constant throughout the length of the beam, the boundary conditions are known as (1) no deflection at the fixed end, (2) the slope is zero at the fixed end, (3) no bending moment acting on

the free end and (4) no shear force acting on the free end. The boundary conditions may be expressed as:

$$Y(0) = 0; \quad Y'(0) = 0; \quad Y''(L) = 0; \quad Y'''(L) = 0 \qquad \textit{Equation 21, 22, 23 \& 24}$$

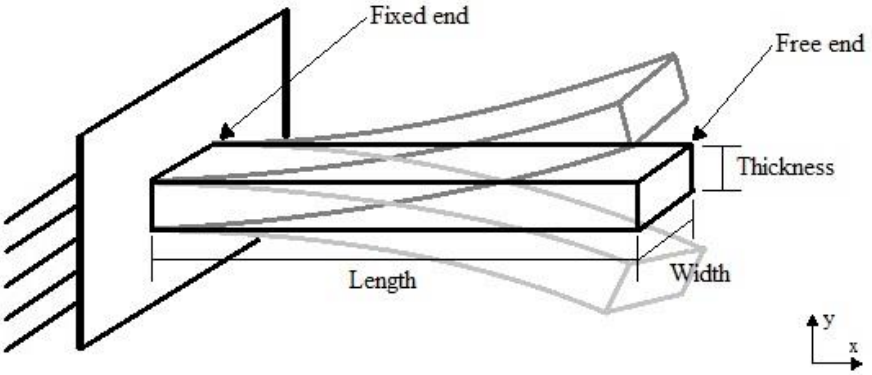

Figure 3 Schematic illustration of a vibrating cantilever beam.

By using the boundary conditions, the following condition is obtained:

$$cos\,\lambda L\, cosh\,\lambda L = -1 \qquad \textit{Equation 25}$$

From equation 25 the value of λ may be determined for each mode of vibration. A schematic drawing of the first three modes are presented in Figure 4 and the value of the first three modes are:

$$(\lambda_1 L) = 1.875$$
$$(\lambda_2 L) = 4.694$$
$$(\lambda_3 L) = 7.855$$

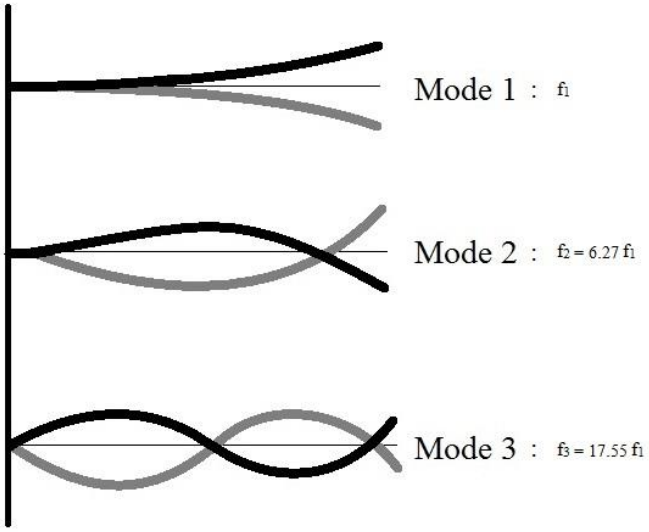

Figure 4 Schematic drawing of the first three modes of vibration.

The circular natural frequency may then be determined as

$$\omega_n = (\lambda_n L)^2 \sqrt{\frac{EI}{\mu L^4}} \qquad \textit{Equation 26}$$

where L is the free length of the beam. Since the natural frequency is obtainable experimentally the modulus of elasticity may be determined by rearranging equation 26.

$$E = \frac{\omega_n^2 \mu L^4}{(\lambda_n L)^4 I} \qquad \textit{Equation 27}$$

2.1.6 Quality factor

The quality factor, Q, is defined as the ratio of the resonance frequency, f_r, over the half-power bandwidth, Δf. The half-power bandwidth is defined as the width of the peak at $1/\sqrt{2}$ of the amplitude at the resonance frequency as illustrated in Figure 5. The equation for the quality factor is expressed as (Thorby, 2008, pp. 108-109)

$$Q = \frac{f_r}{\Delta f} \qquad \textit{Equation 28}$$

The quality factor may also be related to the damping ratio as

$$Q = \frac{1}{2\zeta} \qquad \textit{Equation 29}$$

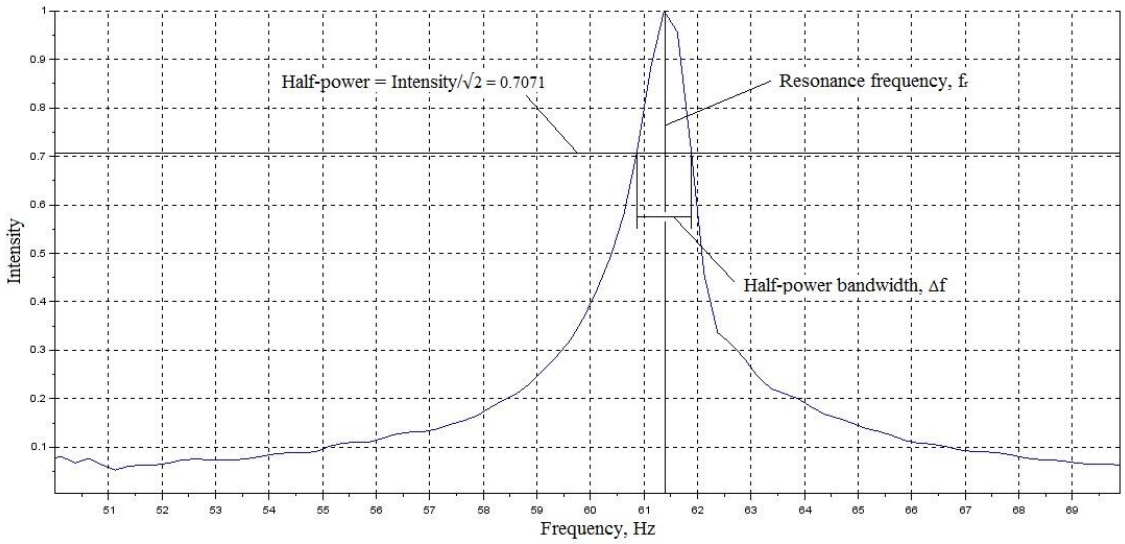

Figure 5 Illustration of the resonance frequency and half-power bandwidth in a frequency spectrum.

2.1.7 Laplace transform and transfer functions

Laplace transform is another method for finding the time response of an excitation to a system, the method also is the basis for the Fast Fourier Transform algorithm. The Laplace transform is used to convert ordinary differential equations into algebraic equations and may in combination with a transfer function and a known input function, define the solution for the output function. (Thorby, 2008, pp. 46-48) (Kelly, 2011, pp. 332-335)

$$\ddot{x} + 2\zeta\omega_n\dot{x} + \omega_n^2 x = \frac{f(t)}{m} \qquad \textit{Equation 30}$$

The equation above is the standard form for forced vibration, where $f(t)$ is the external force acting on the system. The Laplace transform is defined as

$$X(s) = \int_0^\infty e^{-st}x(t)dt \qquad \textit{Equation 31}$$

Where the operator s is defined as

$$s = \sigma + i\omega \qquad \textit{Equation 32}$$

If the real part $\sigma = 0$, the Laplace transform becomes what is called the Fourier transform where $s = i\omega$. Setting the initial conditions to $x = 0$ and $\dot{x} = 0$ and applying the Laplace transform to each term in equation 30,

$$X(s) = \mathcal{L}\{x(t); t \to s\}; \qquad F(s) = \mathcal{L}\{f(t); t \to s\} \qquad \textit{Equation 33}$$

gives

$$(s^2 + 2\zeta\omega_n s + \omega_n^2)X(s) = \frac{F(s)}{m} \qquad \textit{Equation 34}$$

The transfer function, $G(s)$, is a relation between the Laplace transform of the output and input functions of the system.

$$G(s) = \frac{X(s)}{F(s)} = \frac{1}{m} \cdot \frac{1}{(s^2+2\zeta\omega_n s+\omega_n^2)} \qquad \textit{Equation 35}$$

Which may be rearranged to

$$X(s) = G(s)F(s) \qquad \textit{Equation 36}$$

Hence the transfer function and the input function may be used to find the output through the inverse Laplace transform.

$$x(t) = \mathcal{L}^{-1}\{X(s)\} = \mathcal{L}^{-1}\{G(s)F(s)\} \qquad \textit{Equation 37}$$

The input function, defined by the type of excitation is required to determine response. Typical excitation modes are delta impulse, step response and forced sine excitation.

The delta impulse is an excitation mode where the system experiences a sudden change in velocity, in practice, for example, being struck by a moving object. From Table 1 the Laplace transform for a delta impulse may be found to be $F(s) = 1$. As a result the output of a delta impulse reduces to only the inverse Laplace transform of the transfer function. (Thorby, 2008, pp. 50-52)

$$x(t) = \mathcal{L}^{-1}\{G(s)\} = \mathcal{L}^{-1}\left\{\frac{1}{m} \cdot \left[\frac{1}{(s^2+2\zeta\omega_n s+\omega_n^2)}\right]\right\} \quad \textit{Equation 38}$$

Equation 38 may then be solved using Table 1 backwards.

$$x(t) = \frac{1}{m\omega_d}\left(e^{-\zeta\omega_n t}\, sin\, \omega_d t\right) \quad \textit{Equation 39}$$

Where

$$\omega_d = \omega_n\sqrt{1-\zeta^2} \quad \textit{Equation 40}$$

Table 1 Common Laplace transforms. (Thorby, 2008, p. 387)

f(t)	F(s)	Notes
$\boldsymbol{\delta(t)}$	1	Delta impulse
$\boldsymbol{H(t)}$	$\frac{1}{s}$	Step response
$\frac{\mathbf{1}}{\boldsymbol{\omega_d}}\boldsymbol{e^{-\zeta\omega_d t}}\,\mathbf{sin}\,\boldsymbol{\omega_d t}$	$\frac{1}{s^2+2\zeta\omega_n s+\omega_n^2}$	$\omega_d = \omega_n\sqrt{1-\zeta^2}$
$\boldsymbol{e^{-Ct}}\,\mathbf{sin}\,\boldsymbol{\omega t}$	$\frac{\omega}{(s+C)^2+\omega^2}$	
$\boldsymbol{e^{-Ct}}\,\mathbf{cos}\,\boldsymbol{\omega t}$	$\frac{s+C}{(s+C)^2+\omega^2}$	

The step response is the response of a system being displaced by a force, P, and released. From Table 1 it is noticed that $F(s) = \frac{1}{s}$. (Thorby, 2008, pp. 48-50)

$$x(t) = \mathcal{L}^{-1}\{G(s)F(s)\} =$$
$$\mathcal{L}^{-1}\left\{\frac{1}{m} \cdot \frac{1}{(s^2+2\zeta\omega_n s+\omega_n^2)} \cdot \frac{P}{s}\right\} = \mathcal{L}^{-1}\left\{\frac{P}{m}\left[\frac{1}{s} \cdot \frac{1}{(s^2+2\zeta\omega_n s+\omega_n^2)}\right]\right\} \quad \textit{Equation 41}$$

The inverse Laplace transform is in this case not commonly found in tables and need to be split into partial fractions. Noting that $\frac{P}{m}$ is just a constant that can be multiplied to the answer, it does not need to be included in the transform and the equation may be expressed as:

$$\left[\frac{1}{s}\cdot\frac{1}{(s^2+2\zeta\omega_n s+\omega_n^2)}\right] \equiv \frac{A}{s}+\frac{Bs+C}{(s^2+2\zeta\omega_n s+\omega_n^2)} \qquad \textit{Equation 42}$$

A, B and C are constants that need to be found, since equation 42 is an identity valid for any value of s the equation may be rewritten with the intention of finding A, B and C.

$$1 \equiv A(s^2+2\zeta\omega_n s+\omega_n^2)+Bs^2+Cs \qquad \textit{Equation 43}$$

If equating the constants and coefficients of s and s^2 and subsequently substituting for A, B and C back into equation 42 the following equation is obtained.

$$\frac{1}{\omega_n^2}\left[\frac{1}{s}-\frac{s+2\zeta\omega_n}{(s^2+2\zeta\omega_n s+\omega_n^2)}\right] \qquad \textit{Equation 44}$$

The second term in the brackets is still too complex to solve, but may be rewritten if rewriting the denominator first, keeping in mind that $\omega_d = \omega_n\sqrt{1-\zeta^2}$.

$$(s^2+2\zeta\omega_n s+\omega_n^2) = (s+\zeta\omega_n)^2+\omega_d^2 \qquad \textit{Equation 45}$$

Which gives

$$\frac{1}{\omega_n^2}\left[\frac{1}{s}-\frac{s+\zeta\omega_n}{(s+\zeta\omega_n)^2+\omega_d^2}-\frac{\left(\frac{\zeta}{\sqrt{1-\zeta^2}}\right)\omega_d}{(s+\zeta\omega_n)^2+\omega_d^2}\right] \qquad \textit{Equation 46}$$

All the three terms in the brackets may be solved using Table 1 and reinserting the term $\frac{P}{m}$ yields the result:

$$x(t) = \frac{P}{m\omega_n^2}\left[1-e^{-\zeta\omega_n t}\cos\omega_d t-e^{-\zeta\omega_n t}\frac{\zeta}{\sqrt{1-\zeta^2}}\sin\omega_d t\right] =$$

$$\frac{P}{m\omega_n^2}\left[1-e^{-\zeta\omega_n t}\left(cos\,\omega_d t+\frac{\zeta}{\sqrt{1-\zeta^2}}sin\,\omega_d t\right)\right] \qquad \textit{Equation 47}$$

2.1.8 3-Point bending

The flexural properties of plastic materials are defined in ISO standard 178 (ISO 178:2010, 2010). The flexural stress is defined as

$$\sigma = \frac{3FL}{2bh^2} \qquad \textit{Equation 48}$$

where F is the applied force, L is the span length, b is the width and h is the thickness of the specimen.

The flexural strain is defined as

$$\varepsilon = \frac{6yh}{L^2} \qquad \textit{Equation 49}$$

where y is the deflection of the specimen.

A schematic drawing of the principle of three-point bending is presented in Figure 6. The y-axis is inverted as the positive direction of the deflection is downwards and the tip of the indenter marks the zero point.

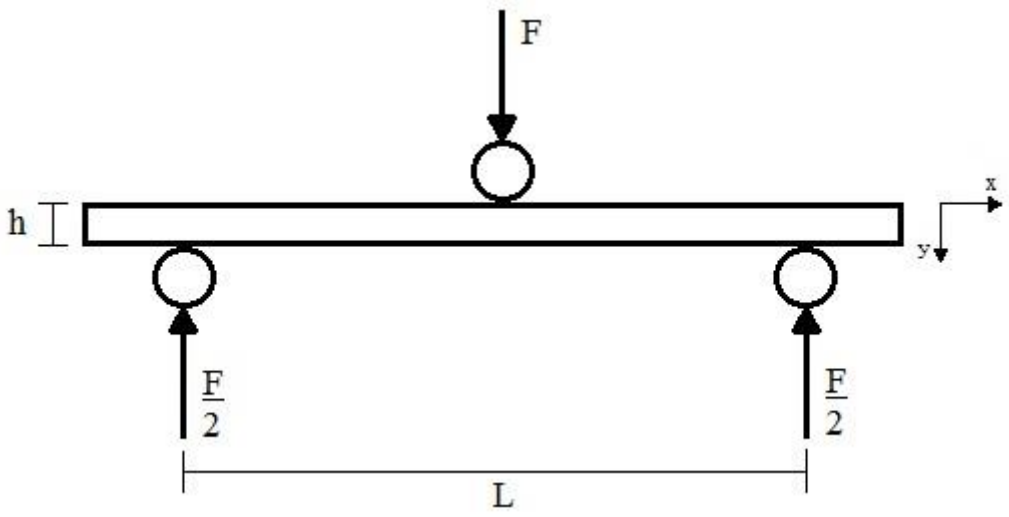

Figure 6 Schematic drawing of the principle of three-point bending.

The flexural modulus may be determined from the stress and strain as illustrated in Figure 7.

$$E = \frac{\Delta\sigma}{\Delta\varepsilon} = \frac{L^3\left(\frac{\Delta F}{\Delta y}\right)}{48I} \qquad \textit{Equation 50}$$

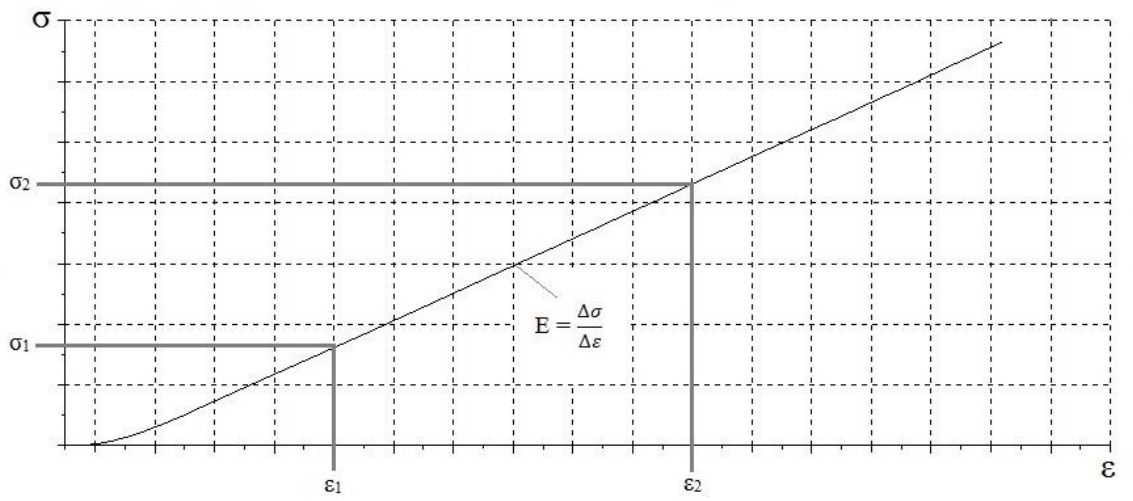

Figure 7 The slope of the stress-strain curve represent the modulus of elasticity.

Important to note is that the area of the hysteresis loop from a loading-unloading 3-point bending cycle is normally seen as the amount of energy dissipated by the material, but a research by Van Paepegem et al. (Van Paepegem, et al., 2006) shows that the friction at the supports significantly affects the result and the area enclosed by the hysteresis loop may not be used as a direct measurement of the energy absorbed.

2.2 Sampling

2.2.1 Software

Audacity is a free open source software for recording live audio and editing of audio files. Audacity will serve as the recording software for the acoustic vibrational tests in this thesis. (Audacity, u.d.)

Scilab is another free open source software, but for numerical computation and offer the possibility compute algorithms and functions for a vast amount of applications such as simulation, optimisation or signal processing. The time series data recorded with Audacity will be computed and visualized as graphs with Scilab. A Fast Fourier Transform algorithm is used to obtain analysable frequency data. (Scilab Enterprises S.A.S, 2015)

2.2.2 Fast Fourier Transform (FFT)

In vibrational tests the data collected experimentally are analogue readings that are continuous points in time, referred to as time series data. The Fast Fourier Transform (FFT) is an algorithm that converts the time series data into Fourier series from which frequency data are obtainable. The frequency data may then be analysed to determine the resonant frequency and half-power bandwidth necessary for the calculation of material properties. (Thorby, 2008, pp. 247-256)

2.3 Failure modes of laminates

The fatigue life of a metal may in most cases be expected to be linear until the fatigue limit is reached. The typical failure mode of laminates subjected to fatigue from bending is however split into three phases as illustrated in Figure 8. (Krüger & Rolfes, 2015) (Sudevan, et al., 2015)

The first phase consists of crack initiation and growth of existing impurities in the matrix as well as matrix-fibre de-bonding. This phase is dominantly logarithmic and accordingly most damage will occur instantly and as the matrix closes in on crack saturation the damage growth will reduce. In this phase buckling may also occur as a result of a pointy or spherical indenter e.g. in 3-point bending, causing local damage to the surface. (Krüger & Rolfes, 2015) (Sudevan, et al., 2015)

The second phase becomes dominant as a result of the matrix having reached crack saturation and the cracks will instead continue to grow along the fibres causing delamination between layers in the laminate. This is a phenomenon happening slowly but steadily, leading to this phase being dominantly linear. (Krüger & Rolfes, 2015) (Sudevan, et al., 2015)

The third and final phase consist of fibre brakeage, ultimately leading to material failure. This phase is dominantly exponential, as fibre brakeage will greatly weaken the material and accelerate the progress. Figure 9 illustrates the three phases of damage accumulation. (Krüger & Rolfes, 2015) (Sudevan, et al., 2015)

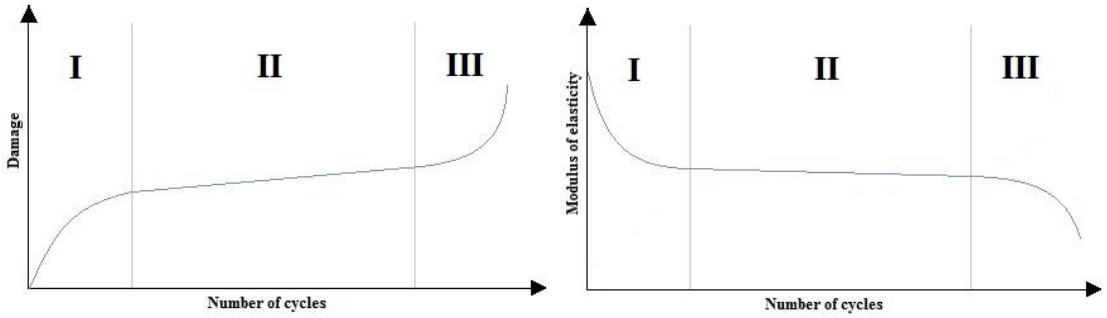

Figure 8 To the left a schematic drawing of the damage accumulation over time to laminates subjected to bending fatigue and to the right the effect of the damage to the modulus of elasticity.

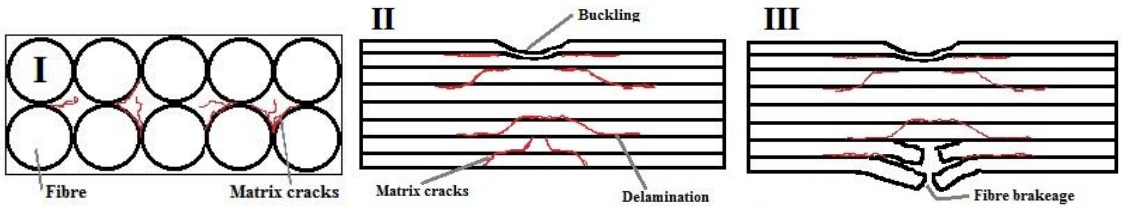

Figure 9 Schematic drawing of the three phases of damage accumulation. (I) Matrix cracking and matrix-fibre de-bonding, (II) delamination and (III) fibre brakeage.

3 METHOD

3.1 Material and specimen preparation

The specimens tested are made of a combination of a unidirectional carbon fibre and a 0°/90° glass fibre with a vinyl ester resin matrix and were manufactured through vacuum bagging and infusion. The process consist of sealing the textile under a plastic film and infusing resin with vacuum pressure applied under the plastic film, this is schematically illustrated in Figure 10. This means that with perfect vacuum the pressure put on the laminate would be equal one atmosphere (~101 kPa). The specimens were prepared to rectangular pieces using a band saw, with the unidirectional carbon fibre in the length direction (0°) of the specimen. The stacking sequences of the laminas are presented in Table 2 and schematically in Figure 11. The specifications of the specimens are presented in Table 3.

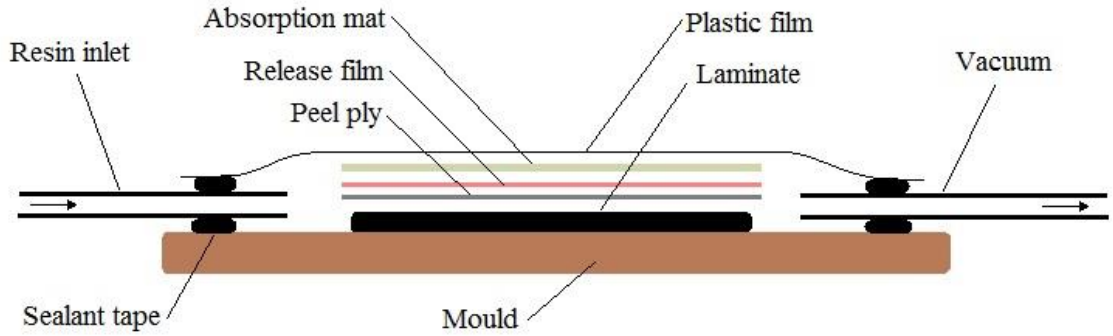

Figure 10 Schematic drawing of vacuum bagging with resin infusion.

One of the two laminates prepared has its layers sewed together with cotton thread in the z-direction, perpendicular to the unidirectional carbon fibres, to form a laminate with fibres in three dimensions. The purpose of this is an attempt to resist delamination to spread as the material ages. By adding fibres to the laminate in a direction other than the direction of stress, the strength-to-weight ratio of the laminate will be lowered, but with the expected benefit of making the material more resistant to fatigue.

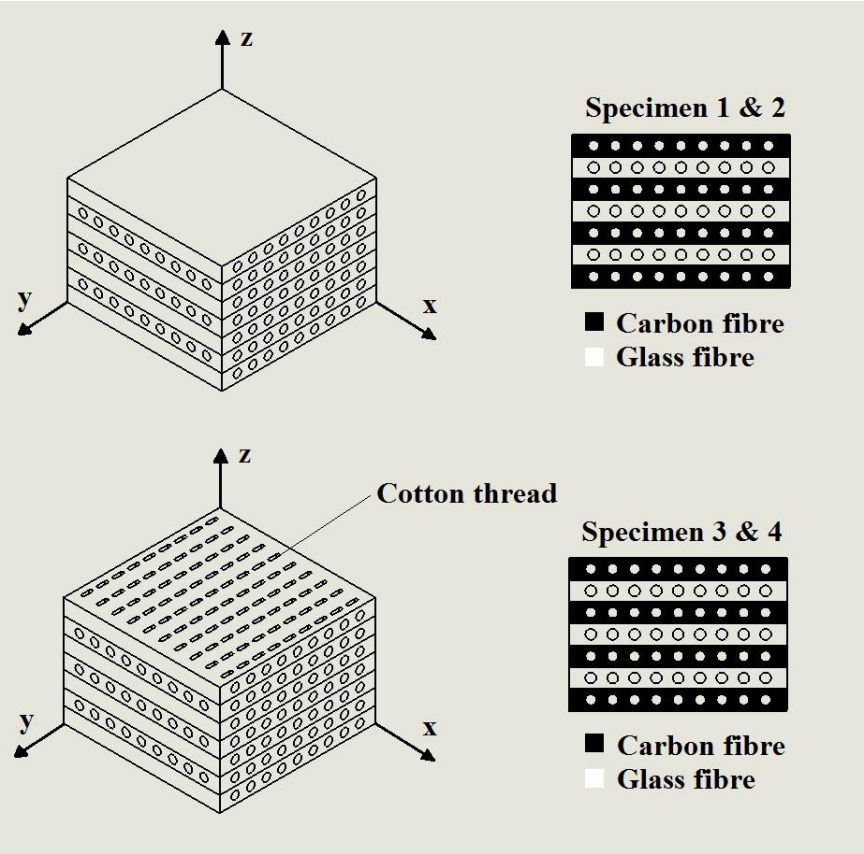

Figure 11 Schematic drawing of the stacking order and fibre orientation of the specimens.

Table 2 Stacking sequence and materials of the laminates.

Laminate		Layer 1	Layer 2	Layer 3	Layer 4	Layer 5	Layer 6	Layer 7	z-direction
1	Material	Carbon fibre	Glass fibre	Carbon fibre	Glass fibre	Carbon fibre	Glass fibre	Carbon fibre	-
	Percent of fibres in x/y-direction	100/0	50/50	100/0	50/50	100/0	50/50	100/0	
2	Material	Carbon fibre	Glass fibre	Carbon fibre	Glass fibre	Carbon fibre	Glass fibre	Carbon fibre	Cotton thread
	Percent of fibres in x/y-direction	100/0	50/50	100/0	50/50	100/0	50/50	100/0	

Table 3 Specifications of the specimens.

Specimen	Laminate	Mass, g	Thickness, mm	Length, mm	Width, mm
1	1	11.38	1.646	202	24.53
2	1	11.13	1.582	202.5	24.62
3	2	12.99	1.88	202.5	25.15
4	2	12.49	1.886	202.5	24.09

3.2 Sampling

3.2.1 Setup for 3-point bending

The ageing of the specimens were performed by causing fatigue degradation to the material by high strain cyclic 3-point bending. The apparatus used was a material testing machine (Testometric M350-5CT) for 3-point bending with a maximum load capacity of 5 kN. In cyclic tests the maximum velocity for the machine is 100 mm/min, with a maximum of 999 cycles per set. The specimen lays on cylindrical supports with a span of 75 mm and the cylindrical indenter is centred between the supports. The indenter and the supports both have a diameter of 10 mm. Stoppers were attached to the ends of the supports to stop the specimens from gliding sideward along the supports during the tests. The gap between the stoppers and the specimen was roughly 1 mm on each side, to ensure specimens were still able to freely move. The setup is shown in Figure 12.

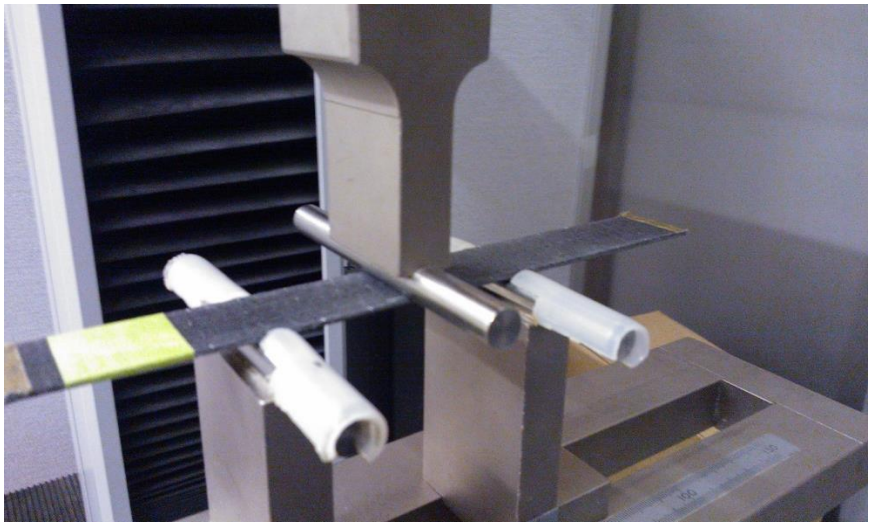

Figure 12 Material testing machine for cyclic 3-point bending.

3.2.2 Setup for vibrational testing

For this thesis the hysteretic damping is the damping mode of interest, but it will not likely be the only damping present. A problem is that each form of damping contributing to the measured damping cannot be distinguished from each other. This means that the measured damping will in fact be a combination of all present damping in the system. Thus it is necessary to eliminate or keep the other forms of damping constant, in that way the

only change in damping will be originating from hysteretic damping as a result of ageing to the material.

The viscous damping may for example be omitted in vacuum, but would lead to acoustic testing being unusable as well. Since the dimensions of the specimen and the medium (air) may be considered to be constant throughout the tests, the only factors affecting the viscous damping are the amplitude and velocity of the vibrations. If the induction of motion to the system is to be made identical for each sample, the amplitude and velocity should accordingly be identical for each individual sample. The induction of motion is in this case done manually and is therefore challenging to get identical. However, with a setup from which the specimen may be released from the same position each time, the viscous damping may be considered to be constant throughout the tests as well. If frictional damping is considered very small compared to the hysteretic damping, the only change in damping or at least the major part of the change should then be originating from hysteretic damping. As the material ages the influence of frictional damping may however increase, as delamination occurs in the laminate.

The vibrations were recorded acoustically with a microphone (Microsoft LifeChat LX-1000) placed beneath the vibrating specimen and the recordings were processed with the software Audacity. The clamping device consists of two steel plates in which between the specimen is fixed and a large steel plate extending backwards as a counterweight as shown in Figure 13.

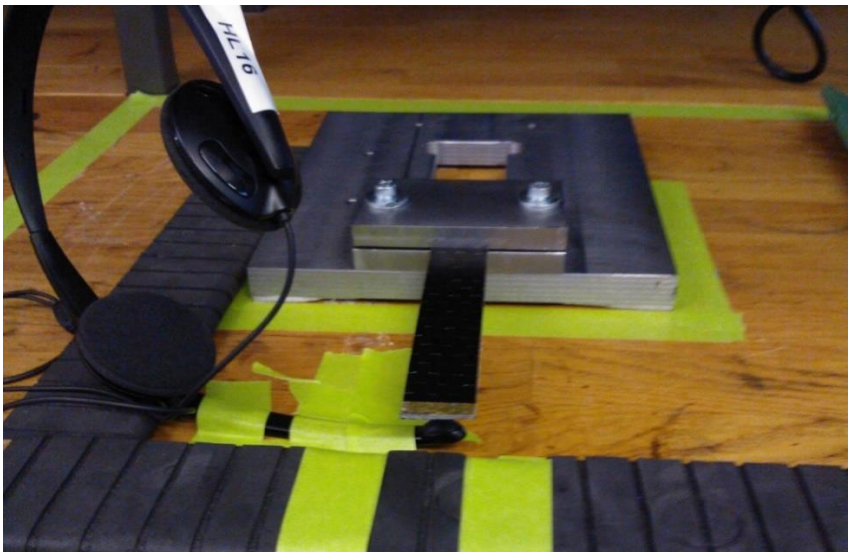

Figure 13 The clamping device for a cantilever beam and the microphone placement.

3.2.3 Ageing of the material and the gathering of data

To inflict damage to the material the specimens were put under constant amplitude cycling for sets of 999 cycles at a velocity of 100 mm/min for 10 sets or a total of 9990 cycles. Specimen 1 and 3 were aged at 0.8 % strain and specimen 2 and 4 at 1 % strain. The strain limit of carbon fibre is 1.8 % and the strain levels of the carbon fibres in the test is thus 44 % and 55 % of the strain limit, which was considered to be enough to cause major damage to specimen in form of resin cracking and delamination but not enough to cause the specimen to brake prematurely. The amplitudes needed to cause the desired strain was calculated according to equation 49.

The code presented in Appendix A was used to calculate the slope for each individual cycle, by inputting the raw data gathered. In this case the slope represent the modulus of elasticity as shown in equation 50. The modulus of elasticity was then plotted against the number of cycles to define the change over time. The expected results are that the force necessary for displacing the specimen will decrease as the material ages and accordingly also the modulus of elasticity. The expected nature of the results are presented in Figure 14.

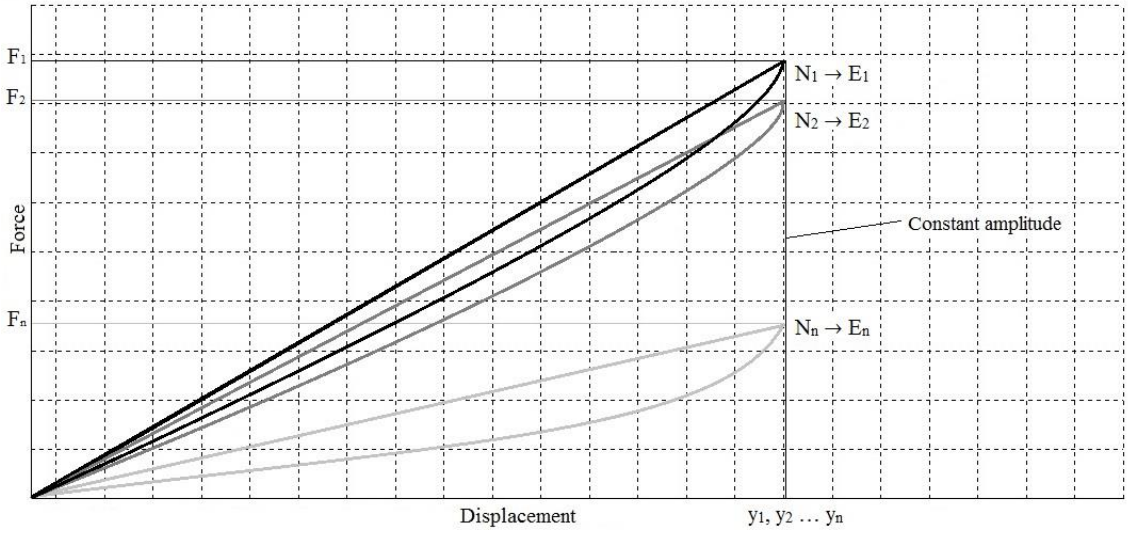

Figure 14 Schematic illustration of the expected change to the force and modulus of elasticity due to ageing.

3.2.4 Vibrational tests and the gathering of data

Vibrational tests were performed on the specimens in their initial condition before ageing the material and after every following set of 999 bending cycles, with 25 samples recorded

for each test. The vibrations were induced manually by displacement of the specimen using a plastic stick. The stick was placed on a fixed support from which the specimen could be displaced and was removed horizontally away from the specimen in an attempt to make the induction identical for each sample. The data was collected using the recording software Audacity at a sample rate of 8000 Hz and mono recording. The parameters used when recording are presented in Figure 15.

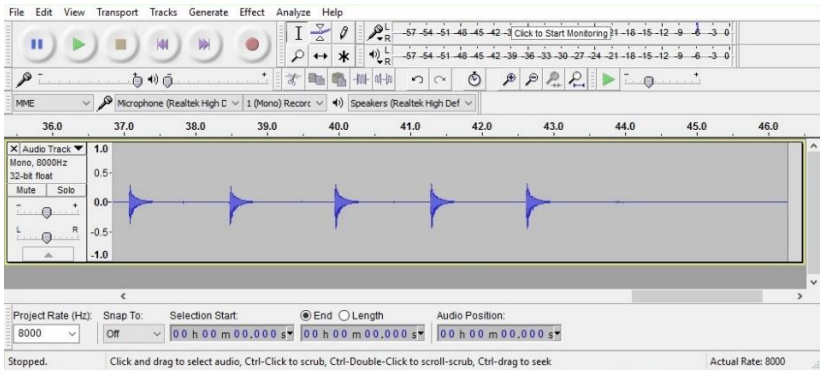

Figure 15 Screenshot of Audacity including the parameters used for acoustically recording the vibrations.

The code presented in Appendix B was run in the software Scilab. The code is using the Fast Fourier Transform to transform the vibrational time data into a frequency spectrum as shown in Figure 16. The resonance frequency and half-power bandwidth was obtained by analysing the frequency spectrum. This information, along with the specifications of the specimens, were used to determine the modulus of elasticity and quality factor according to equation 27 and equation 28 respectively. The systematic tests allowed for the values of the modulus of elasticity and the quality factor to be plotted against the number of cycles to witness the change over time.

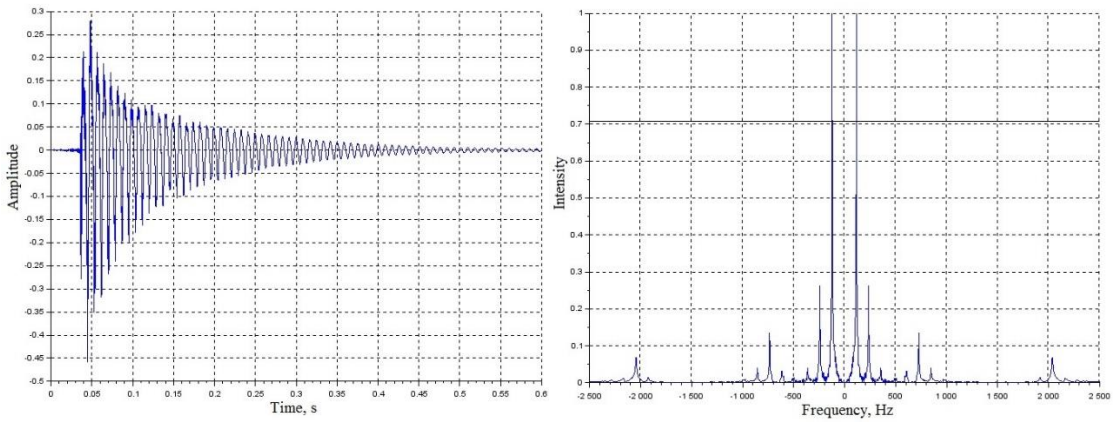

Figure 16 Example of the time data plot and frequency spectrum from the undamaged specimen 2.

Only the first mode of vibrations are of interest for this thesis as it is the dominant mode for this particular case. The peak of the first mode in this sample is at approximately 120 Hz as seen in Figure 16 and it is undoubtedly the dominant peak in this spectrum. The two following peaks are at 240 Hz and 360 Hz and are overtones of the first peak. At roughly 730 Hz is the peak of the second mode of vibrations and at roughly 2040 Hz is the peak of the third mode of vibrations. The resonance frequency of mode 2 and 3 are very close to the theoretical values, which are 6.27 and 17.55 times the resonance frequency of mode 1, respectively.

The expected results are that the resonance frequency, and consequently the modulus of elasticity, will decrease as the material ages. Similarly it is expected that the half-power bandwidth will increase, resulting in a decrease in the quality factor, as the material ages. This phenomenon is presented in Figure 17.

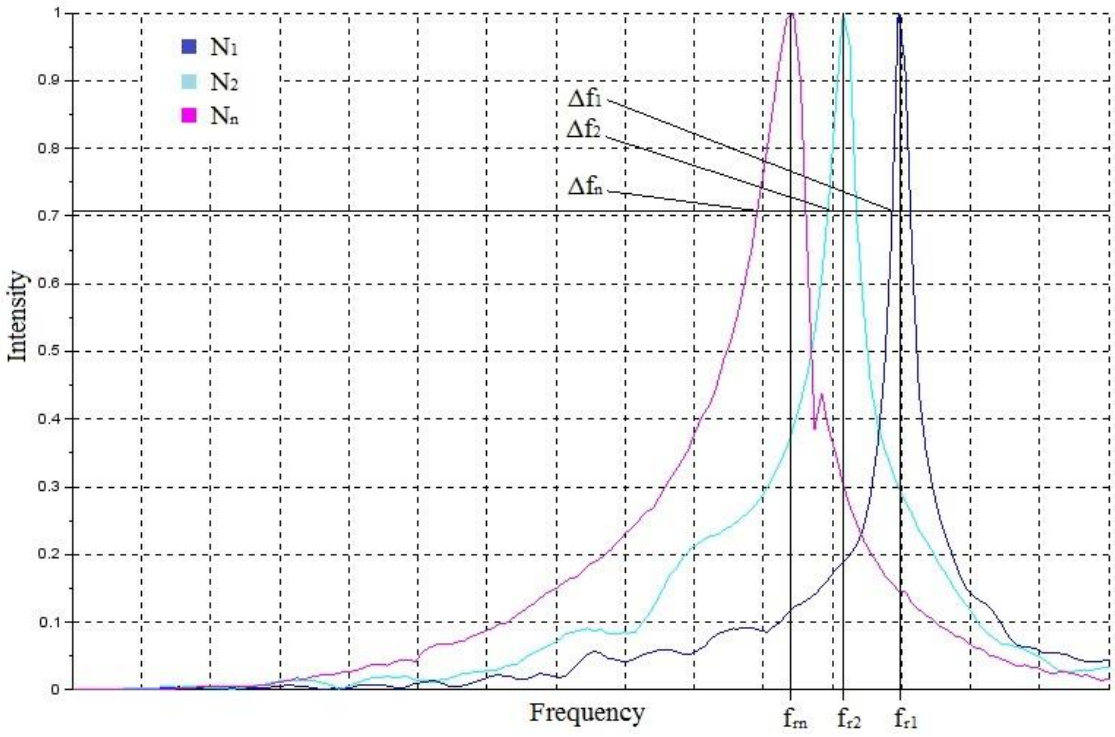

Figure 17 Schematic illustration of the expected change to the resonance frequency and half-power bandwidth due to material ageing.

4 RESULTS

4.1 Bending test results

The data collected during the ageing of the specimens are presented in force-displacement graphs in Figure 18. If the force is great enough to damage the specimen, each cycle will generate a loop as described in section 2.1.3. The graph is consisting of hysteresis loops from each of the 9990 cycles, for each of the specimens. An important notion is that the exact amount of energy dissipated cannot be determined from the loop as the result is highly depending on the friction at the supports. The specimens were tested at constant amplitude cycling meaning the displacement was constant during the tests and as such the expected result is that the force needed to displace the specimen will be reduced as the specimen weakens as a result of fatigue. This phenomenon is clearly visible in the graphs as the loops tend to become more and more horizontal as the damage grows. This is expected as the modulus of elasticity is represented by the slope as described in equation 50 and a steeper slope indicates a higher modulus of elasticity.

Analysing the results indicates that there was most damage to the specimens at the early stages as the drop of the cycles in the beginning are greater than at later stages, this is especially visible in specimen 2, 3 and 4. Specifically specimen 4 took much damage at the very first cycle and a visible sudden drop, moments before reaching the set deflection, is likely a result of fibres breaking, which could be a result of buckling at the bending point.

As mentioned the slope is a representation of the modulus of elasticity and was plotted for each individual cycle to get a visual of the change over time, the results are presented in Figure 19. As expected the result is logarithmically decaying, the initial damage is great, but the damage growth quickly reduces and especially for specimen 1 and 3 there is very little damage growth showing in the later stages. Specimen 2 and 4 were subjected to higher strain and show more damage growth in the later stages, indicating that more delamination have occurred in those specimens. Comparing the results between the 2D and 3D laminates, it seems that the 3D laminates shows less damage growth in the later

stages, which may be a sign of resistance to delamination spreading across the laminate due to the extra fibres in the z-direction.

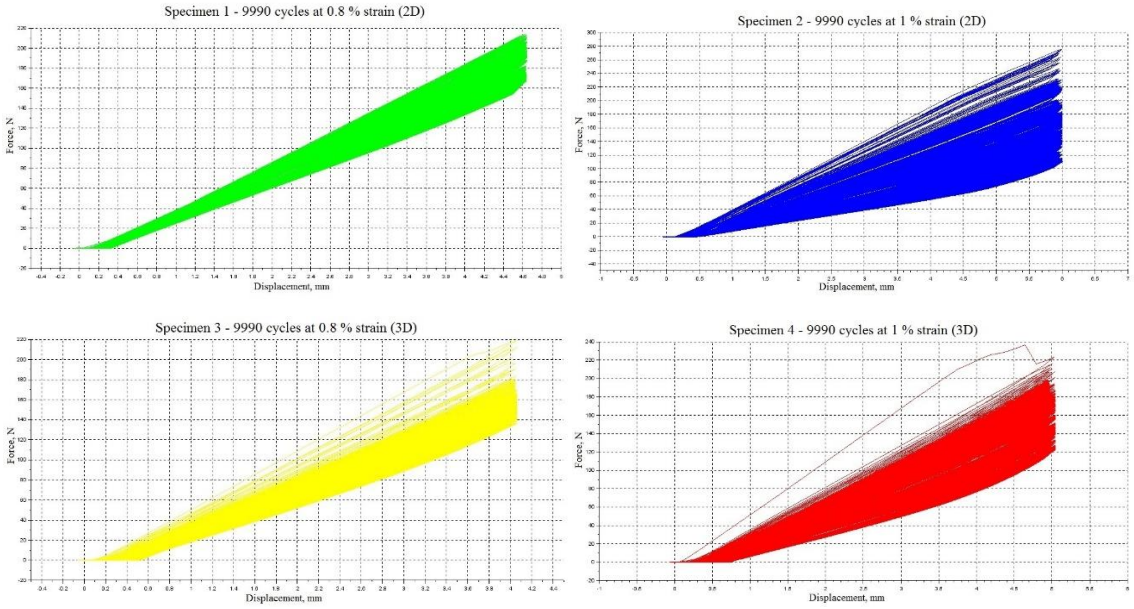

Figure 18 Hysteresis loops as a result of ageing to the specimens, where the slope represent the modulus of elasticity.

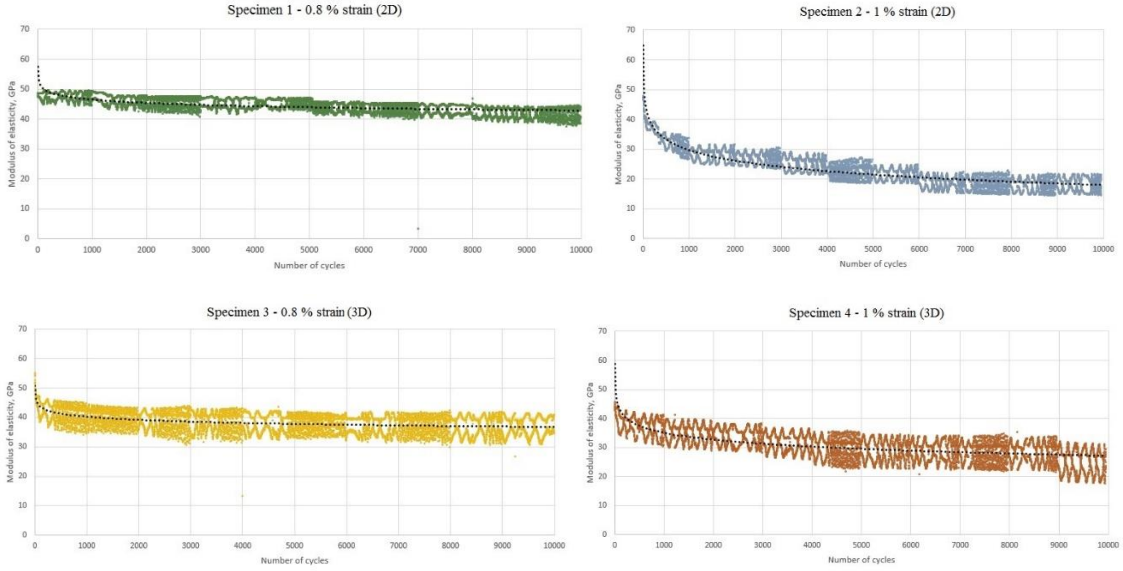

Figure 19 The change of the modulus of elasticity versus the number of cycles.

The large variation visible in Figure 19 is entirely due to bugs in the code that fail to define the start and end of a cycle, an example of this error is shown in Figure 20. The software calculates the linear average of the data supplied and with an error, such as shown in Figure 20, the calculated slope is to some extent offset and not a representation

of the actual slope. Since the slope represent the modulus of elasticity, the calculated value will be offset accordingly. Therefore it is very important that these values is not treated as exact numbers. The trend line however shows an accurate representation of the relative damage to the specimen and may be used as a tool for predicting damage accumulation and material failure.

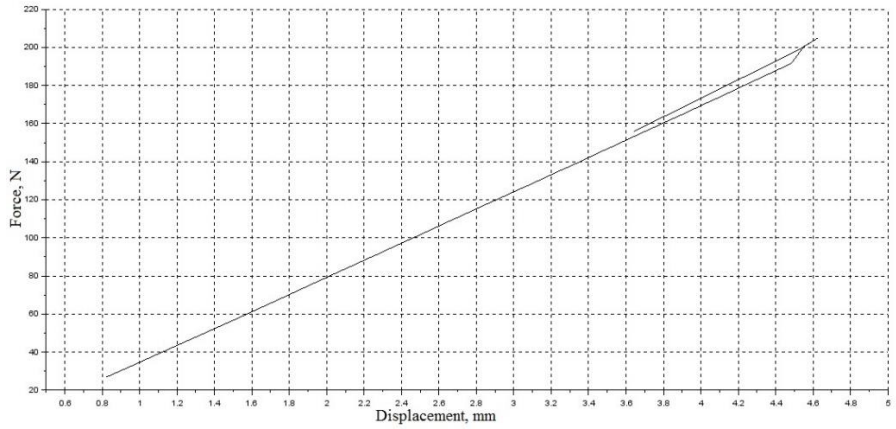

Figure 20 Example of an error defining the slope due to a bug in the code.

4.2 Vibrational test results

The results of the vibrational tests are presented in Figure 21, where the left column shows the modulus of elasticity and the right column shows the quality factor both versus the number of cycles. As each specimen were tested before ageing and after every set of 999 cycles up to ten full sets and each vibrational tests consisted of 25 samples. The variation between samples in individual tests were typically very small as seen in Table 4. The modulus of elasticity, calculated from the resonance frequency according to equation 27, had very little to no variation between samples. The variation on undamaged and slightly damaged specimens was mainly due to precision errors in the software offsetting the resonance frequency by exactly 1 Hz. As the specimens got more damaged the resonance peak tended to get wider, which resulted in the peak being increasingly more round-tipped instead of pointy, causing minor variations to the highest point on the peak between samples. The quality factor, calculated from the ratio between the resonance frequency and half-power bandwidth of the peak according to equation 28, had more variation between samples as a result of approximation errors made by the software. The software only calculates data points and when plotting a graph the software make straight lines between these points, which is not the true representation of the curve.

Table 4 Range of relative variations for the modulus of elasticity and the quality factor of the four specimens.

Specimen		**1**	**2**	**3**	**4**
Relative variations	**E**	0 - 0.21 %	0 - 0.38 %	0.16 – 0.38 %	0 – 0.72 %
	Q	0.63 - 2.27 %	1.30 - 3.74 %	1.86 – 3.72 %	0.04 – 4.06 %

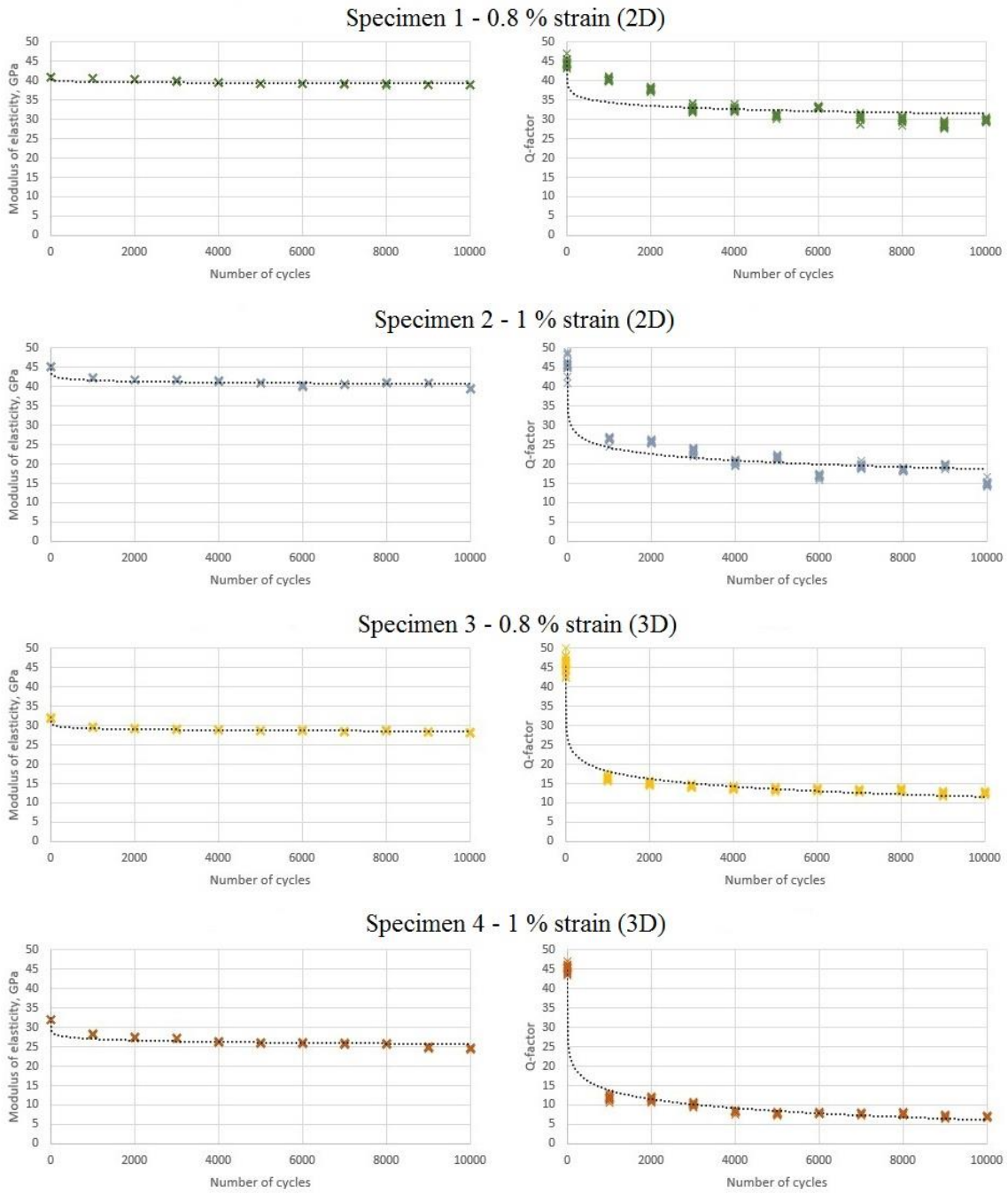

Figure 21 The left column shows the change of the modulus of elasticity versus the number of cycles and the right column shows the change of the quality factor versus the number of cycles.

Studying the curves in Figure 21, shows a clear logarithmically decaying tendency, which is the expected result as described in section 2.3 describing the failure modes of laminates. As the initial damage growth is predominantly in the matrix, the fibres remain mostly undamaged in the early stages of the damage accumulation. Since the modulus of elasticity is to a great extent dependent on the fibres rather than the matrix, the decrease should be relatively small although still following a logarithmically decaying pattern. As clearly seen in Figure 21 this is also the case where most damage occur between 0 and 1000 cycles. Even that damage only cause a minor decrease to the modulus of elasticity. Noteworthy is that the value of the modulus of elasticity differs from the values measured during bending.

The quality factor is in contrast to the modulus of elasticity depending on the quality of the matrix and should similarly show a logarithmic decay, but with a great initial decrease as the damage accumulation in the matrix is dominant in early stages of the fatigue life and slows down as the matrix approaches its point of crack saturation. Comparing the expectations to the curves in Figure 21 it is seen that the decrease is at its greatest between 0 and 1000 cycles. The rate of damage growth is also far more rapid than the damage growth later on, indicating that the matrix is approaching its point of crack saturation even before the first set of 999 cycles.

Comparing the results of the 2D and 3D laminates it is noticeable that the 3D laminates, specimen 3 and 4, have a much greater initial decrease of the quality factor than the 2D laminates as seen in Figure 21. This is likely a result of damage concentration at the bending point, as the additional fibres in the z-direction of the 3D laminates may hinder damage to spread across the laminate. The effect of the additional fibres in the z-direction on the spreading and growth of damage is proved by analysing the second phase of damage accumulation, which is delamination. The second phase is shown in Figure 22 and Figure 23, which shows the same results as Figure 21 excluding the first 1000 cycles resulting in the slope being dominantly linear for that region.

As seen in Figure 22 there is not much variation between the specimens, all four having only a slight decrease in the modulus of elasticity. This is expected as the second phase of damage accumulation is dominantly due to delamination in the laminate. Delamination

leaves the fibres mostly undamaged and accordingly does not remarkably affect the modulus of elasticity either as the fibres are the main contributor to the modulus of elasticity. Noticeable is that the value of the modulus of elasticity is 21.8 % – 29.5 % lower for the 3D laminate, specimen 3 and 4, compared to the 2D laminate, specimen 1 and 2. This is expected as well, as the additional fibres in the z-direction made the laminate thicker without adding any strength to the direction of stress. Another likely reason is that the carbon fibres might have gotten damaged when sewn together, further weakening the 3D laminate.

Figure 23 shows the linear region of the quality factor versus the number of cycles and from the slope it is evident that the decrease is slower for the 3D laminates. The 2D laminates, specimen 1 and 2, both have the quality factor decreasing with 0.0011 per cycle, while the 3D laminates, specimen 3 and 4, have the quality factor decreasing with 0.0004 and 0.0005 per cycle respectively. This proves that the addition of fibres in the z-direction in fact resist the spreading and growth of delamination in the laminate. The ageing was slowed down by 54.5 % and 63.6 % for specimen 3 and 4, respectively, compared to their 2D laminate equivalents, by the addition of cotton thread in the z-direction.

The correlation between the modulus of elasticity and the quality factor is shown in Figure 24. From the graph it is apparent that the relationship is linear, proving that the modulus of elasticity and quality factor may be predicted if the slope is known. The decrease of the quality factor is however much greater than for the modulus of elasticity, which further proves that, at least, for the early stages of ageing the quality factor is a better tool for measuring the ageing as the damage is mostly concentrated in the matrix rather than in the fibres.

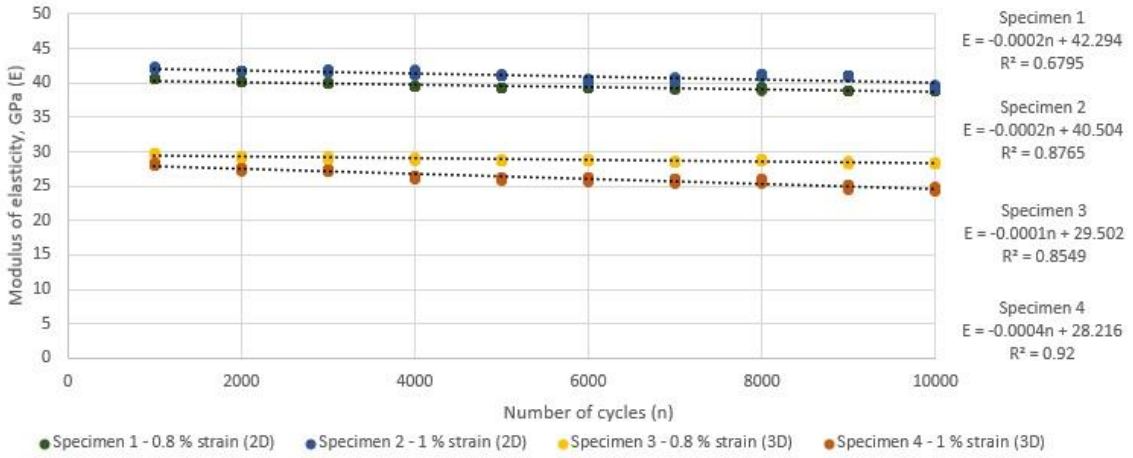

Figure 22 The linear region of the modulus of elasticity versus the number of cycles.

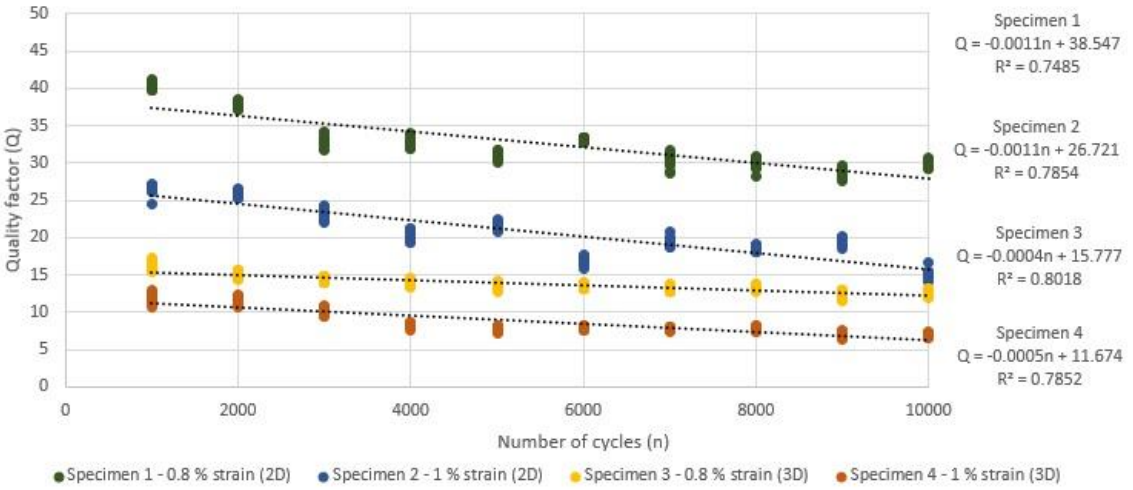

Figure 23 The linear region of the quality factor versus the number of cycles.

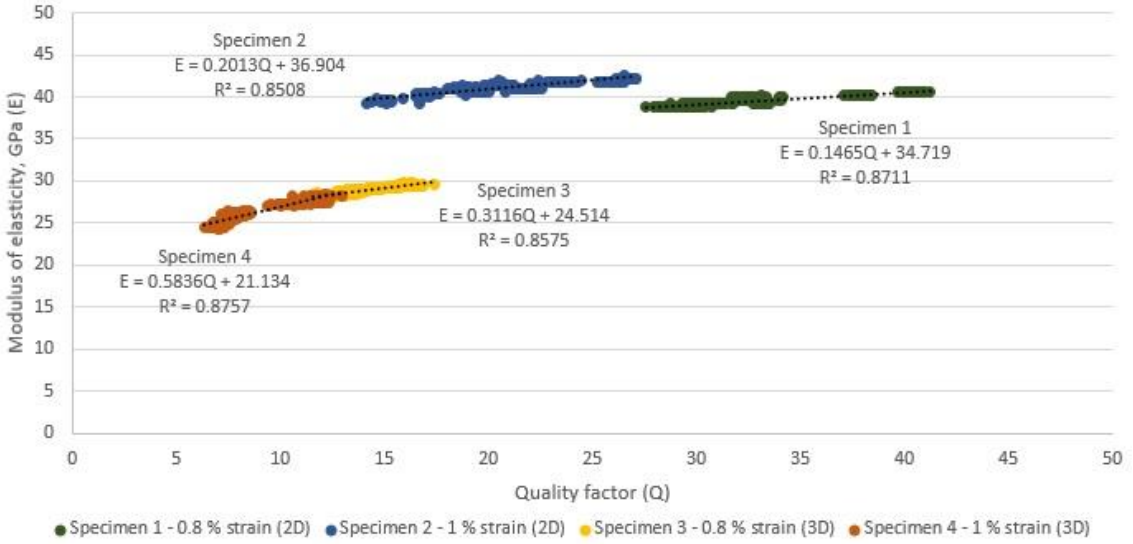

Figure 24 The relationship between the modulus of elasticity and the quality factor as a result of ageing.

4.3 Damage analysis

The most noticeable visible damage is large cracks in the direction of the unidirectional carbon fibres in specimen 1 and 2 as seen in Figure 25 and Figure 26 respectively. These cracks are a result of matrix-fibre de-bonding and occurred already after the first set of cycles. Specimen 3 and 4 on the other hand shows more local damage of several shorter and smaller cracks forming around the stiches from the thread in the z-direction shown in Figure 27 and Figure 28 respectively. The stiches from the thread in the z-direction is observed distorting the fibres in Figure 30 which shows the smooth side of specimen 3 and 4. These distortions will have stress concentrations formed around them as the specimens is put under stress which explains why the visible damage is primarily close to the stiches.

Marked in red in Figure 25 – 28 are visible points where fibre brakeage has occurred as a result of buckling due to compression. Figure 31 shows an example of visible buckling and delamination during bending, a phenomenon which occurred in all four specimens. Comparing the damage of the side subjected to compression seen in Figures 25 – 28 and the side subjected to tension seen in Figure 29 – 30 it is evident that the side subjected to tension has next to none visible damage, while the side subjected to compression have a combination of matrix cracking and fibre brakeage as already described. Comparing specimen 1 and 3 to specimen 2 and 4 it is noticeable that the latter have more visible damage, which is expected as specimen 2 and 4 were subjected to greater strain.

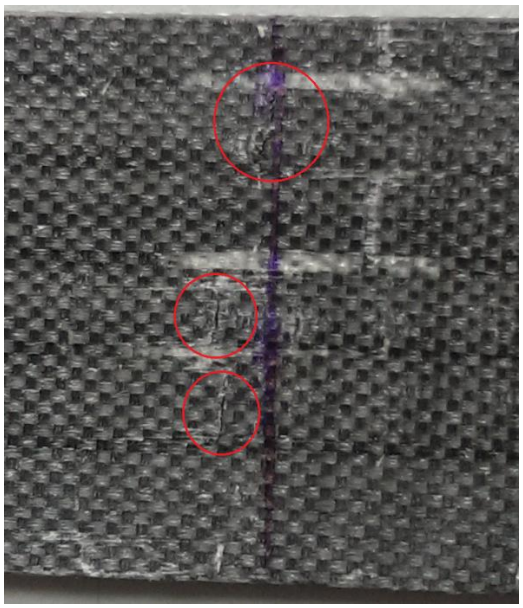

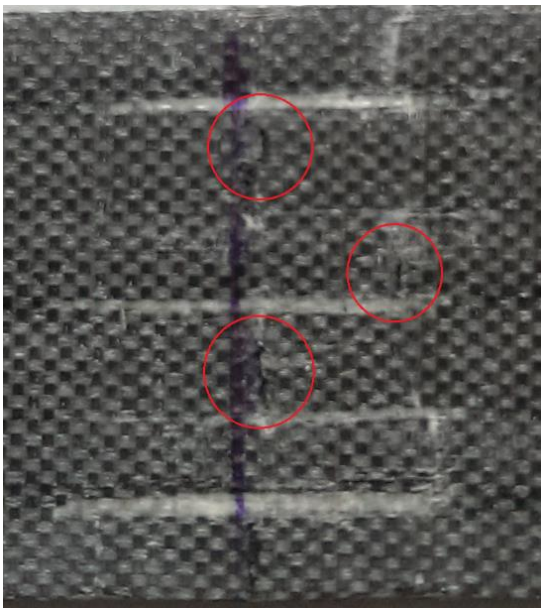

Figure 25 To the left specimen 1, damage due to compression.

Figure 26 To the right specimen 2, damage due to compression.

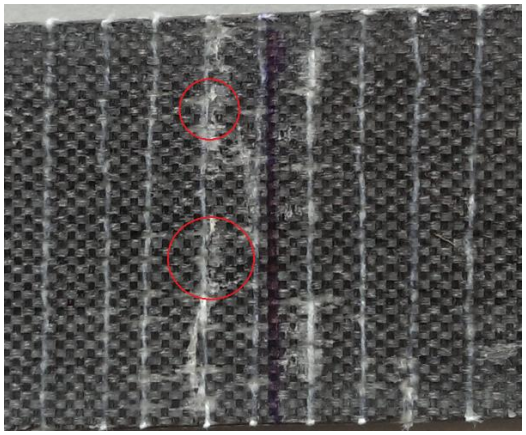

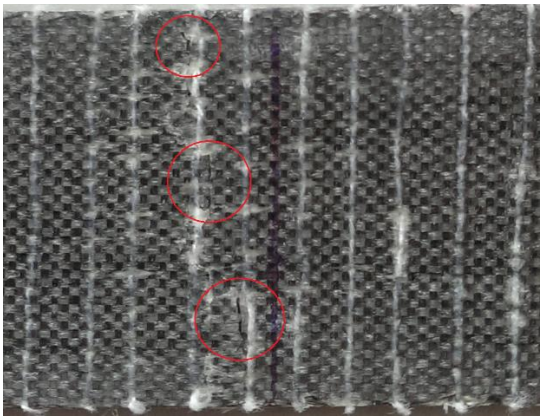

Figure 27 To the left specimen 3, damage due to compression.

Figure 28 To the right specimen 4, damage due to compression.

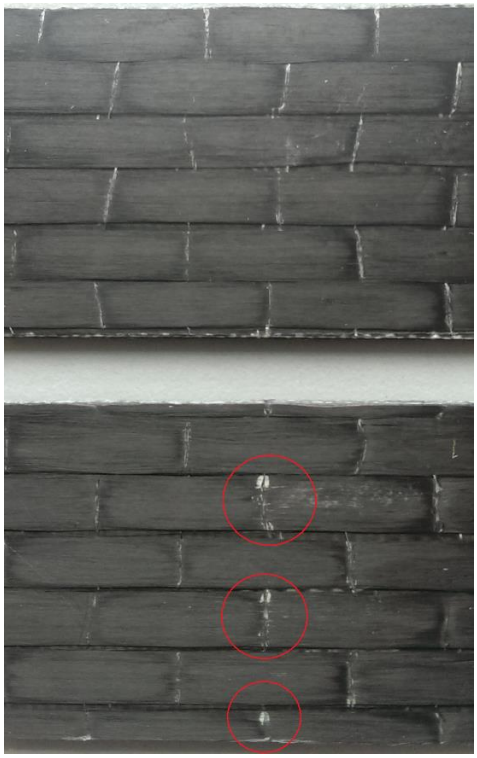

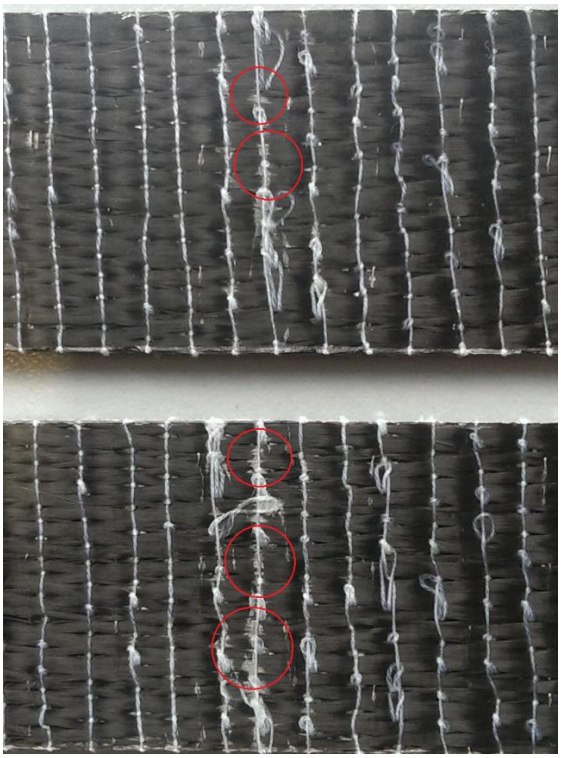

Figure 29 To the left specimen 1 & 2, damage due to tension.

Figure 30 To the right specimen 3 & 4, damage due to tension.

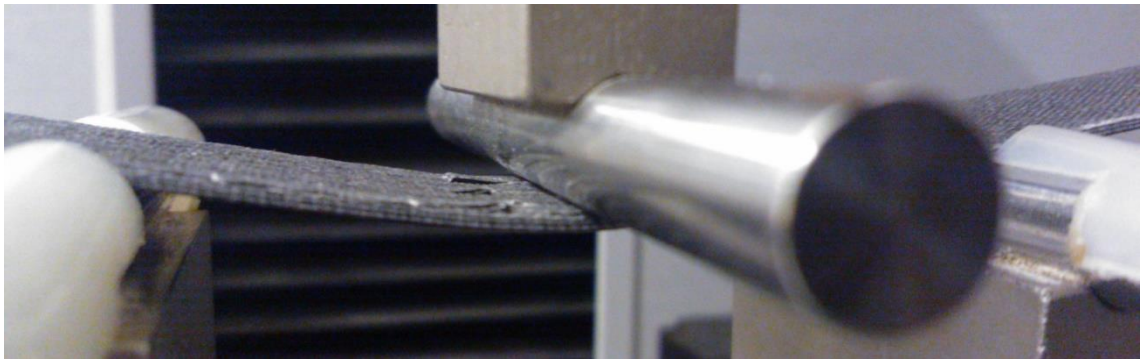

Figure 31 Visible buckling with resulting delamination of the top layer of specimen 2.

5 DISCUSSION

The lamination method chosen for this thesis was vacuum bagging and infusion, although other methods such as heat pressing pre-preg fibres would have likely given a better laminate in terms of fibre volume ratio and even thickness. Vacuum bagging is however a commonly used method for lamination and the method was considered being an easy and appropriate way of achieving a suitable representation of laminates commonly used in terms of quality. The laminates had some thickness variations over the surface, most notably as specimen 1 and 2 has a thickness difference between the averages of 0.064 mm or about 4 %. This is because of the specimens was cut from different ends of the larger laminate and is as such a representation of the thickness variation across the whole laminate. The thickness variation of the individual specimens were considerably lower.

The layup could arguably have been made up of merely the unidirectional carbon fibre, but the glass fibre was considered adding stability between layers as the higher strain limit of the glass fibre had it stay intact and therefore offered great contrast in terms of colours, aiding in the analysis of visible damage.

To achieve best results from comparing 2D and 3D laminates, a woven 3D textile would unquestionably be recommended instead of simply stitching a 2D textile stack together. Although the self-made 3D textile in theory should achieve the same results, there will certainly be imprecisions such as stiches covering more than, or less than, one string of textile in the x/y-direction. This would result in the fibres not being perfectly symmetrically stacked as well as the risk of damaging fibres while sewing, which will reduce the strength and quality of the lamina.

Specimen preparation should ideally be done by laser or water jet cutting to achieve straight and clean edges without damaging the specimen. The method chosen for this thesis was however cutting by band saw, due to availability and simplicity of the method. Cutting by band saw may however include the risk of causing damage to the specimens such as delamination at the edges as well as being considerably more inaccurate than an automated cutting method.

An alternative method to cyclic three-point bending are four-point bending, which work by the same principle as three point bending but have two indenters. This would cause the damage to be more even and spread over a larger area, which might be a more realistic approach to material damage. However as the vibrations are measured with a cantilever setup, it is actually more desirable having local damage that is easy to localise.

The limiting factor in the method chosen is actually not in three-point bending but in the speed that the machine operates at. A maximum testing speed of 100 mm/min, led to that the specimens were only tested at 9990 cycles, but at relatively high strains to achieve enough damage with that few cycles. To achieve a full understanding of the fatigue life it would be necessary to accomplish possibly million cycles or more. At 100 mm/min a million cycles are beyond reach unless the deflection would be exceptionally small. A proper fatigue testing machine capable of operating at hundreds of Hertz, would allow for the specimen to be tested at lower strains and at more cycles. This may be a more accurate representation of the damage a part may receive under its lifetime, as well as a greater part of its fatigue life.

A method for vibrational analysis often preferred is a fixed-fixed or free-free setup where the vibrations are induced using a hammer. Neither of those were chosen for this thesis as the method were a cantilever setup where the vibrations were induced by offsetting the free end. Both methods were however considered, but testing the methods showed that the fixed-fixed clamping device available was not robust enough and vibrations from the clamping device itself interfered with the vibrations of the specimen. The free-free setup was yet challenging for keeping the specimen in place. Induction of vibrations were also tested using a hammer, with the conclusion that manually hitting the exact same spot was problematical and led to greater variation in the results than manually offsetting the cantilever beam. Having a robust fixed-fixed clamping device and an automated device for the induction of vibrations may nevertheless be a superior testing method.

The codes used for this thesis could undoubtedly be improved, but with the of lack time, the codes were limited to the essentials necessary for getting analysable results. Most important for this study was however the damage trend or the relative damage rather than exact results.

6 CONCLUSIONS

The results indicate that the specimens were noticeably damaged as a result of ageing from cyclic three-point bending and the value of the quality factor was determined to be an accurate representation of the damage accumulation in the laminate. As most damage occur in the matrix in the early stages of ageing, the quality factor gave a better representation of the damage growth, as the modulus of elasticity is strongly related to the strength of the fibres. The correlation between the quality factor and modulus elasticity was nevertheless proven to be linear.

The relative variation of the quality factor reach up to 4 % in the tests, which may be too much variation to usefully determine the condition of the material. If the test were made with more accurate equipment, as discussed in the previous chapter, the variation may be reduced to such a level that the information could be used to accurately determine the damage and possibly more accurately predict the remaining life of the material. The conclusion is nevertheless that acoustic vibrational analysis is a suitable method for non-destructively determine the ageing of fibre-reinforced plastics.

The point of material failure may not be determined from the results of this thesis as the number of cycles were far too few. The specimens were still prone to damage growth at 9990 cycles and may as such be expected to continue decreasing linearly until initiation of fibre brakeage and ultimately material failure. There is however possible that the damage growth would stop completely and continue without taking further damage, resulting in the specimen never reaching material failure. This thesis consequently fail to confirm the applicability of regular acoustic vibrational tests as a method of predicting material failure. To confirm this hypothesis it would be recommended that in further research use high frequency fatigue testing equipment that allows for a larger number of cycles. This would provide a more accurate definition of the fatigue life of fibre-reinforced plastics.

The quality factor furthermore proved that 3D laminates have a remarkable effect on resisting spreading and growth of damage in laminates compared to their 2D laminate equivalents. The addition of cotton thread in the z-direction slowed down the spreading

and growth of damage by 54.5 % – 63.6 %. The drawback was that the modulus of elasticity for the 3D laminates were reduced by 21.8 % – 29.5 %.

The failure modes due to fatigue damage were determined by analysing the visible damage to the surface of the specimens. Matrix cracks were the most noticeable damage, where the 2D laminates had large cracks in the direction of the unidirectional carbon fibres indicating matrix-fibre de-bonding, while the 3D laminate had cracks mainly around the stiches of the fibres in the z-direction. Some cases of fibre brakeage were noticed on all four specimen, which were concluded to be a result of buckling from the cylindrical indenter. These failure modes were all textbook examples, which further confirms that the damage accumulation can be predicted for fibre-reinforced plastics, at least in the early stages.

REFERENCES

Ajaja, J. & Barthelat, F., 2016. Damage accumulation in a carbon fiber fabric reinforced cyanate ester composite subjected to mechanical loading and thermal cycling. *Composites Part B,* Volume 90, pp. 523-529.

Audacity, n.d. *About Audacity.* [Online]
Available at: http://audacityteam.org/about/
[Accessed 3 December 2015].

Backe, D., Balle, F. & Eifler, D., 2015. Fatigue testing of CFRP in the Very High Cycle Fatigue (VHCF) regime at ultrasonic frequencies. *Composites Science and Technology*, Volume 106, pp. 93-99.

Capozucca, R., 2014. Vibration of CFRP cantilever beam with damage. *Composite Structures,* Volume 116, pp. 211-222.

El Messiry, M., 2013. Theoretical analysis of natural fiber volume fraction of reinforced composites. *Alexandria Engineering Journal,* Volume 52, pp. 301-306.

ISO 178:2010, 2010. *Plastics - Determination of flexural properties.* 5 ed. Geneva: International Organization for Standardization.

Kelly, S. G., 2011. *Mechanical Vibrations: Theory and Applications.* Stamford(CT): Cengage Learning.

Krüger, H. & Rolfes, R., 2015. A physically based fatigue damage model for fibre-reinforced plastics under plane loading. *International Journal of Fatigue,* Volume 70, pp. 241-251.

Safa, B. C., Mehmet, T. A. & Baki, Ö., 2011. Transverse Vibration Analysis of Euler-Bernoulli Beams Using Analytical Approximate Techniques. In: E. Farzad, ed. *Advances in Vibration Analysis Research.* 1st ed. s.l.:InTech, pp. 1-22.

Scilab Enterprises S.A.S, 2015. *About Scilab.* [Online]
Available at: http://www.scilab.org/scilab/about
[Accessed 3 December 2015].

Sudevan, D., Prakash, R. V. & Kamaraj, M., 2015. Post-impact Fatigue Response of CFRP Laminates under Constant Amplitude and Programmed FALSTAFF Spectrum Loading. *Procedia Engineering,* Volume 101, pp. 395-403.

Thomson, W. T., 1996. *Theory of Vibration with Applications.* 4th ed. Cheltenham: Taylor & Francis Ltd.

Thorby, D., 2008. *Structural Dynamics and Vibration in Practice.* 1st ed. Oxford: Butterworth-Heinemann.

Van Paepegem, W., De Geyter, K., Vanhooymissen, P. & Degrieck, J., 2006. Effect on friction on the hysteresis loops from three-point bending fatigue tests of fibre-reinforced composites. *Composite Structures,* 72(2), pp. 212-217.

Xue, H. Q. et al., 2007. Development of a three-point bending fatigue testing methodology at 20 kHz frequency. *International Journal of Fatigue,* Volume 29, pp. 2085-2093.

Xue, L.-Z.et al., 2015. Flexural fatigue behaviour of 2D cross-ply carbon/carbon composites at room temperature. *Materials Science & Engineering A,* Volume 634, pp. 209-214.

Yan, Y. J., Cheng, L., Wu, Z. Y. & Yam, L. H., 2007. Development in vibration-based structural damage detection technique. *Mechanical Systems and Signal Processing,* Volume 21, pp. 2198-2211.

Yan, Y. J., Yam, L. H., Cheng, L. & Yu, L., 2006. FEM modeling method of damage structures for structural damage detection. *Composite Structures,* Volume 72, pp. 193-199.

Zhang, Z. et al., 2013. Vibration-based inverse algorithms for detection of delamination in composites. *Composite Structures,* Volume 102, pp. 226-236.

APPENDICES

Appendix A - Fatigue analysis code

```
A=fscanfMat('filename.txt');
F=A(:,2);
x=A(:,1);

//Graph of fatigue, Force vs. displacement

xset("window",0)
xgrid(0)
plot2d(x,F,5)
xlabel('Displacement')
ylabel('Force')
title('All cycles')

//Definition of data

dx=diff(x);
L=find(dx>0); //All data for the load cycle
R=find(dx<0); //All data for the return cycle

dx_L=diff(L);
dx_R=diff(R);
int_L=find(dx_L>1); //Start and End values of load cycles
int_R=find(dx_R>1);

//Defining the slope

Range=[1:9990]; //All intervals
N=2;
```

```
Intervals=Range(2:N:length(Range)); //Only intervals for loading cycle

marginal=0; //Trimming the ends for access of only the slope

a=0:1:max(size(int_L));
a=a*0;

for i=Intervals(1:4995);
F_L=F((int_L(i)+marginal):(int_L(i+1)-marginal*3));
x_L=x((int_L(i)+marginal):(int_L(i+1)-marginal*3));
[a(i),b,sig]=reglin(x_L',F_L');

//Slope

xset("window",1)
xgrid(0)
plot2d(x_L,F_L,i)
xlabel('Displacement')
ylabel('Force')
title('Slope')
end

//Plotting Young's modulus vs. number of cycles

xset("window",2)
xgrid(0)
plot(a)
xlabel('Number of cyles')
ylabel('Youngs modulus')
title('Fatigue')
```

Appendix B - FFT code

```
D = fscanfMat('filename.csv');

dt=1/8000;
T_max=max(size(D));
t=0:1:T_max-1;
t=t*dt;

//compute the fft
y=fft(D,-1);
spektrum=fftshift(abs(y));

//display
xset("window",0)
xgrid(0)
plot2d(t,D,2)

hans=spektrum/inttrap(spektrum);

xset("window",1)
xgrid(0)
frequency=0:1/max(t):(max(size(t))-1)/max(t);
niva=0*frequency+0.7071;

plot2d(frequency-0.5*max(frequency),hans/max(hans),2)
plot2d(frequency-0.5*max(frequency),niva,1)
```